# A Time-Frequency Local Polynomial Approach to FRM Estimation from Incomplete Data

Dirkx, Nic; Tiels, Koen; Oomen, Tom

**DOI**
10.1016/j.ifacol.2023.10.1332

**Publication date**
2023

**Document Version**
Final published version

**Published in**
IFAC-PapersOnLine

Available online at www.sciencedirect.com

ScienceDirect

IFAC Papers Online CONFERENCE PAPER ARCHIVE

IFAC PapersOnLine 56-2 (2023) 3942–3947

# A Time-Frequency Local Polynomial Approach to FRM Estimation from Incomplete Data ⋆

**Nic Dirkx** [*,**] **Koen Tiels** [**] **Tom Oomen** [**,***]

[*] *ASML Research Mechatronics & Control, Veldhoven, The Netherlands*

[**] *Eindhoven University of Technology, Department of Mechanical Engineering, Control Systems Technology, Eindhoven, The Netherlands*

[***] *Delft Center for Systems and Control, Delft University of Technology, Delft, The Netherlands*

**Abstract:** Frequency Response Matrix (FRM) estimation from measured data is an important step towards the control of complex systems, including motion and thermal systems. Missing samples in the measured data records, e.g., due to sensor failure or faulty data transmission, often occur. In this paper, a method is presented for the nonparametric FRM identification of multiple-inputs multiple-outputs (MIMO) systems from incomplete and noisy data records. The method exploits time- and frequency-domain localizing wavelets to accurately estimate the FRM and its covariance from the time-frequency plane. Good performance is demonstrated in a simulation study.



*Keywords:* Frequency response function identification, missing data, transient estimation, multiple-inputs multiple-outputs, linear systems

## 1. INTRODUCTION

Nonparametric FRM identification from experimental data is a crucial aspect in the design, control, and analysis of dynamical systems. Particularly for highly complex systems, including closed-loop controlled MIMO motion and thermal systems, FRM identification is considered simple, fast, and accurate (Schoukens et al., 2009).

The handling of leakage errors is an important aspect in nonparametric FRM identification. Among different FRM identification approaches, including the spectral analysis (SA) and empirical transfer function estimate (ETFE) (Pintelon and Schoukens, 2012, Ch. 2), the Local Polynomial Method (LPM) (Pintelon et al., 2010) is particularly effective in handling leakage errors, by exploiting the fact that leakage is induced by transient phenomena that exhibit smooth frequency-domain characteristics.

In many practical cases, and especially for large MIMO systems generating a large amount of data, the data cannot be obtained uninterruptedly, which gives rise to missing samples in the measured data record. Missing samples may also originate from sensor or communication link failure (Kar and Moura, 2009). The presence of locally missing samples introduces a global perturbation in the frequency-domain (Ugryumova et al., 2014), which complicates the estimation problem.

Existing approaches to nonparametric FRM identification with missing data aim at reconstruction of the missing parts, and involve the estimation of additional parameters. In Barbé et al. (2012), a spectrum reconstruction is performed by estimating an additional transient contribution per missing data part. In Schoukens et al. (2012), a similar principle is applied in an extension of the classical LPM framework. Since the number of estimated transients increases with the number of data gaps, the methods become infeasible for an increasing number of data gaps.

Alternative reconstruction approaches consist in including the missing samples as additional estimation parameters. In Stoica et al. (2009), the missing samples are estimated via an iterative spectrum reconstruction scheme, but the approach is not formulated within a system identification setting. In Ugryumova et al. (2014), the missing samples are included as additional unknowns in an extended LPM. The large-dimensional problem becomes intractable when many missing samples are present.

Departing from reconstruction approaches, prior work Dirkx et al. (2022, 2023) extends the LPM to an identification approach in the time-frequency plane, which enables separating the effects of the missing samples in the time domain from the system frequency response in the frequency domain. The framework is limited to SISO open-loop systems, and does not provide an quantification of the estimation uncertainty.

Although important progress is made in FRM identification, approaches for MIMO closed-loop controlled systems that can feasibly handle many or large missing data parts are lacking. The aim of this paper is to present a method for the nonparametric FRM estimation of closed-loop controlled MIMO systems and their variance from data records with missing samples, by extending upon the results in Dirkx et al. (2022, 2023). Periodic excitation signals are considered.

The main contributions of this paper are:

1. An extension of the wavelet-based LPM for FRM estimation from incomplete data in Dirkx et al. (2022, 2023) to MIMO systems operating in closed-loop,
2. A procedure for estimating the covariance in the estimated FRM from incomplete data,
3. A validation of the techniques in a simulation study.

⋆ This work was supported by the Research Programme VIDI under Project 15698, partly financed by the NWO.


10.1016/j.ifacol.2023.10.1332

*Notations* Operations $x\mathcal{F} = X$ and $X\mathcal{H} = x$ denote the Discrete Fourier Transform (DFT) of $x$ and the inverse DFT (IDFT) of $X$, with $\mathcal{F}$ and $\mathcal{H}$ the DFT and IDFT matrix (Pintelon and Schoukens, 2012, Ch. 2), respectively. Operator $\otimes$ denotes the Kronecker product. For a vector-valued $X$, operation $[X]_n$ selects the $n$-th entry, whereas for matrix-valued $X$ operation $[X]_{n,n}$ selects the $n$-th diagonal entry. Zero-based numbering is applied, unless otherwise noted. Furthermore,

$$\text{blkdg}(X_0, \dots, X_{n-1}) = \begin{bmatrix} X_0 & & \\ & \ddots & \\ & & X_{n-1} \end{bmatrix}.$$

## 2. PROBLEM FORMULATION

### 2.1 FRM identification with missing data

Consider the closed-loop identification setup in Fig. 1, where $G$ represents the $n_y \times n_u$ to-be-identified LTI system, and $C$ is a stabilizing LTI controller. Signal $w^{[e]} \in \mathbb{R}^{n_u \times NP}$ is an $N$-periodic excitation signal, for $P \geq 2$ periods, applied during an $e$-th identification experiment, where $e = 1, \dots, n_u$. The output $y^{[e]}$ is perturbed by noise $\nu^{[e]}$, characterized as a filtered random sequence.

The DFT of $z^{[e]} := \begin{bmatrix} u^{[e]T} & y^{[e]T} \end{bmatrix}^T$ is given by

$$Z^{[e]}(k) = G_z(\Omega_k) W^{[e]}(k) + T_z^{[e]}(\Omega_k) + N_z^{[e]}(k). \tag{1}$$

Herein, the transfer function $G_z$ is given by

$$G_z : w \mapsto z := \begin{bmatrix} G_y \\ G_u \end{bmatrix} = \begin{bmatrix} G \\ I \end{bmatrix} (I + CG)^{-1}. \tag{2}$$

The argument $\Omega_k = e^{-1i \cdot 2\pi k/(NP)}$ is the discrete frequency with $k = 0, \dots, NP-1$. Term $W^{[e]} \in \mathbb{C}^{n_u \times NP}$ is the DFT of $w^{[e]}$. Term $T_z^{[e]}$ is the transient due to the difference between the initial and the final system conditions. The DFT of the noise contribution $\nu^{[e]}$ onto $z^{[e]}$ is governed by $N_z^{[e]}(k) = N_{z_{\text{st}}}^{[e]}(k) + T_h^{[e]}(\Omega_k)$, where $N_{z_{\text{st}}}^{[e]}(k) = H_z(\Omega_k) E^{[e]}(k)$ with $H_z(\Omega_k)$ the monic noise dynamics, $E^{[e]}$ is the DFT of a random noise realization, and $T_h$ is the transient due to the difference between the initial and the final conditions of the noise dynamics.

Suppose that a number of $n_{\text{m}}^{[e]}$ samples is missing in the measurement $z^{\text{m}[e]}$ of the output $z^{[e]}$. Assuming that the indices of the missing samples are known, the measurement is expressed as $z^{\text{m}[e]} = z^{[e]} \mathcal{M}^{[e]}$, where

$$[\mathcal{M}^{[e]}]_{n,n} = \begin{cases} 1 \text{ if sample } n \text{ is available} \\ 0 \text{ if sample } n \text{ is missing} \end{cases}, \tag{3}$$

with $n = 0, \dots, NP-1$. Also see Fig. 1.

Locally missing samples in the time domain have a global impact in the frequency domain. This is evident from the DFT of $z^{\text{m}[e]}$, given by

$$Z^{m[e]} = Z^{[e]} \mathcal{T}^{\text{m}[e]}, \tag{4}$$

where matrix $\mathcal{T}^{\text{m}[e]} = \mathcal{H}\mathcal{M}^{[e]}\mathcal{F}$ becomes non-diagonal when samples are missing. This implies that the principle of frequency-separation is no longer valid when samples are missing, which complicates the use of traditional FRM estimation approaches that rely on this principle, including SA, ETFE, and LPM (Pintelon and Schoukens, 2012).

The main goal of the method presented in this paper is to generate an accurate nonparametric FRM of $G(\Omega_k)$ in (2) including its variance $\text{cov}(\text{vec}(G(\Omega_k)))$ from the incomplete closed-loop data $z^{\text{m}}$.

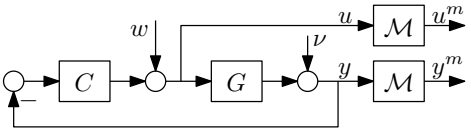


Fig. 1. Closed-loop identification setup with plant $G$, controller $C$. Matrix $\mathcal{M}$ incorporates the structure of the missing samples.

### 2.2 Key idea: time-frequency plane LPM

The classical LPM (Pintelon et al., 2010) is an effective approach for nonparametric FRM estimation in the presence of transients $T_z$, see (1). The main concept that is exploited in the LPM is that the transient is a smooth function of the frequency, and hence in a local frequency window it can be described approximately by a linear-in-the-parameters low order polynomial model. The LPM estimation consists in solving the plant parameters $G_z$ and the polynomial coefficients via least squares minimization based on local frequency-domain information. In Fig. 2(a), an example of a DFT $Z$ (—) and the LPM estimate $\hat{Z}$ (—) is shown. Herein, both the stationary response $G_z(\Omega_k)W^{[e]}(k)$ and transient response $T_z$ are accurately estimated.

When missing samples are present, the locality and smoothness properties on which the LPM relies no longer apply, recall (4), and hence the classical LPM no longer provides a viable approach. This is exemplified in Fig. 2(b), where the missing data is reflected by the DFT $Z^{\text{m}}$ (—). Clearly, the LPM estimate (—) based on $Z^{\text{m}}$ is a poor estimate of the underlying response $Z$ (—).

In this paper, this shortcoming of the classical frequency-domain LPM is addressed by approaching the estimation problem in the two-dimensional time-frequency plane. The key point is that the time-frequency plane representation enables characterizing the frequency response as function of time. As such, it enables separating the effect of the missing samples along the time dimension from the FRM characteristics along the frequency dimension. This is illustrated for the example data $Z^{\text{m}}$ in Fig. 2(c). Herein, the effect of the missing samples is isolated in the part (■) along the time axis. The time-frequency plane LPM aims to estimate the FRM of $G(\Omega_k)$ from the part in (■) that is unaffected by the missing samples. The algorithm is formalized in the next section.

## 3. TIME-FREQUENCY PLANE LPM

### 3.1 Regression model

The key idea of the method is to cast the estimation problem as a linear regression problem in the time-frequency plane, that is insensitive to the missing data.

Consider the frequency-domain input-output relation (1), and let the matrix $Z$ be composed of the data of $n_u$ experiments as $Z = \begin{bmatrix} Z^{[1]}, \dots, Z^{[n_u]} \end{bmatrix}$. Matrices $Z^{\text{m}}, T_z, \bar{K}$, and $N_{z_{\text{st}}}$ are structured likewise. Using that $Z^{\text{m}} = Z + (Z^{\text{m}} - Z)$, the regression model with missing samples is of the form

$$Z^{\text{m}} \bar{M} = \left( \bar{\Theta} \bar{K} + \bar{\mathcal{O}} + N_{z_{\text{st}}} + (Z^{\text{m}} - Z) \right) \bar{M}. \tag{5}$$

Herein, $\bar{\Theta}$ are the real-valued estimation variables that describe the plant $G_z$ and the plant and noise transient $T$, and $\bar{K}$ reflects the assumed model structure. Term $\bar{\mathcal{O}}$ contains higher order dynamics that are not encompassed by the model structure in $\bar{K}$. Explicit expressions for all

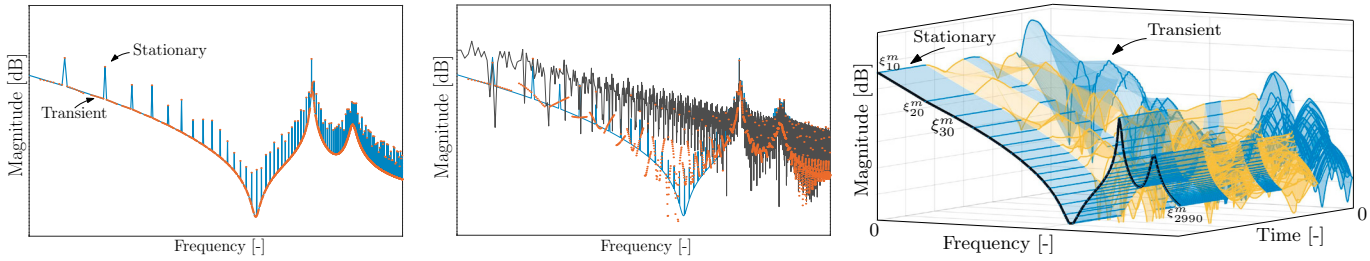


(a) The classical LPM estimate $\hat{Z}(k) = \hat{G}(\Omega_k)W(k) + \hat{T}_z(\Omega_k)$ (—) provides an accurate estimate of the true response data $Z$ (—).

(b) The incomplete data $z^{\mathrm{m}}$ has a non-smooth DFT $Z^{\mathrm{m}}$ (—). Using $Z^{\mathrm{m}}$, the classical LPM estimate $\hat{Z}(k)$ (—) no longer accurately describes $Z$ (—).

(c) Time-frequency plane representation of the data $z^{\mathrm{m}}$. The effect of the missing samples on the frequency-domain characteristics is isolated in the (■) part. The samples in (■) are associated to the set $\mathcal{D}$.

Fig. 2. Example of LPM estimation of $Z(k) = G(\Omega_k)W(k) + T_z(\Omega_k)$ with and without missing samples.

variables in (5) are provided later. The key point of the regression model (5) lies in the weighting matrix $\bar{M}$ that is employed to address the effect of the missing samples. The following least squares estimator for (5) is considered:

$$\hat{\bar{\Theta}} = \Re(Z^{\mathrm{m}}\bar{B}\bar{K}^H)\left(\Re(\bar{K}\bar{B}\bar{K}^H)\right)^{-1}, \tag{6}$$

where $\bar{B} = \bar{M}\bar{M}^H$. Consider the following result.

*Theorem 1.* (Dirkx et al. (2022)). Assume that $N_{z_{\mathrm{st}}} = 0$ and $\bar{\mathcal{O}} = 0$, such that the true system obeys $Z = \bar{\Theta}\bar{K}$. Then, the estimate $\hat{\bar{\Theta}}$ to (6) is exact, i.e., $\hat{\bar{\Theta}} = \bar{\Theta}$, if:

i) $(Z^{\mathrm{m}} - Z)\bar{M} = 0$,
ii) $\bar{K}\bar{M}$ has full row rank.

Conditions i) - ii) in Thm. 1 formulate the essential requirements for achieving an unbiased estimator of the form (6) in view of the term $(Z^{\mathrm{m}} - Z)$.
The conditions in Thm. 1 impose specific demands on the selection of the parameters in (5). In the next sections, explicit expressions for the matrix $\bar{M}$ in (5) and the parametrization $\{K_{\bar{k}_j}, \Theta_{\bar{k}_j}\}$ are presented.

### *3.2 Incorporating the time-frequency plane transform*

The key point of the presented approach lies in selecting the matrix $\bar{M}$ such that the regression (5) is insensitive to the term $(Z^{\mathrm{m}} - Z)$. This is achieved by incorporating a wavelet convolution to transform the data $z^{\mathrm{m}}$ to the time-frequency plane, by which the effect of the missing samples is separated from the FRM of $G_z$ in (1).

#### *3.2.1. Wavelet convolution*

The time-frequency plane representation is obtained by convolving the data $z^{\mathrm{m}}$ with a short-length oscillation, denoted as the wavelet function $\psi_j$ (Daubechies, 1990).

*Definition 1. The circular convolution $\xi_j^{\mathrm{m}} \in \mathbb{C}^{NP}$ of the signal $z^{\mathrm{m}}$ with the wavelet $\psi_j$ is defined as*

$$\xi_j^{\mathrm{m}}[n] := \{z^{\mathrm{m}} \circledast \psi_j\}[n] := \frac{1}{\sqrt{NP}} \sum_{m=0}^{NP-1} \psi_j[m] \cdot z_{NP}^{\mathrm{m}}[n-m]. \tag{7}$$

*where $z_{NP}^{\mathrm{m}}$ be the $NP$-periodic extension of $z^{\mathrm{m}} \in \mathbb{R}^{1\times NP}$ and sample index $n = [0, \ldots, NP-1]$.*

By the convolution theorem, the transform $\xi_j^{\mathrm{m}}$ obeys the frequency-domain expression

$$\xi_j^{\mathrm{m}} = Z^{\mathrm{m}}\mathrm{diag}(\Psi_j)\mathcal{H}, \tag{8}$$

where $\Psi_j$ is the DFT of $\psi_j$. Evidently, $\Psi_j$ acts as a frequency-domain window upon the data $Z^{\mathrm{m}}$. Hence, the transform $\xi_j^{\mathrm{m}}$ reflects the time-domain behavior of the frequency components of $Z^{\mathrm{m}}$ within the selected window, and thus $\xi_j^{\mathrm{m}}$ provides both time- and frequency-specific information of $Z^{\mathrm{m}}$. This is exploited to make the effect of the missing samples local in $\xi_j^{\mathrm{m}}$, which is achieved via suitable selection of the wavelet. This is considered next.

#### *3.2.2. Wavelet selection*

The selection of a suitable wavelet function $\psi_j$ is crucial to obtain a transform $\xi_j^{\mathrm{m}}$ in (7) that accurately reflects the local frequency content of $z^{\mathrm{m}}$ around the frequency line $j$, and at the same time accurately localizes the effect of the missing samples in the time domain. Perfect localization in the two domains, however, cannot be simultaneously achieved, as stated by the Heisenberg-Gabor uncertainty principle, see e.g. Gröchenig (2001). Therefore, wavelet selection involves a trade-off. In this paper, a type of wavelet is considered that enables localizing the effect of missing samples in the time domain, while achieving accurate localization in the frequency domain.

*Definition 2.* (Dirkx et al. (2023)). *Let $j \in \{\mathbb{N} : j \in [0, NP-1]\}$, and let $\delta \in \{\mathbb{R} : N/(2\delta) \in \mathbb{N}, \delta P \in \mathbb{N}\}$. Then, the wavelet $\psi_j^{[p]} \in \mathbb{C}^{1\times NP}$, $p \in \mathbb{N}$ is defined as*

$$\psi_j^{[p]}[m] = c^{[p]}h^{[p]}[m] \cdot e^{1i\cdot 2\pi\frac{j}{NP}m}, \quad m = 0, \ldots, NP-1.$$

*Herein, $c^{[p]} = (\delta\sqrt{P/N})^p$ is a scaling constant and $h^{[p]} = \mathcal{H}(\mathcal{F}h)^p$, with superscript $p$ the element-wise exponent. Function $h$ constitutes the rectangular function*

$$h[m] = \begin{cases} 1 \text{ if } m \leq N/\delta \\ 0 \text{ otherwise} \end{cases}.$$

Consider the following result.

*Lemma 2.* (Dirkx et al. (2023)). *The wavelet function $\psi_j^{[p]}$ in Def. 2 satisfies the following properties:*

*a) $\Psi_j^{[p]} = 1$ at the $j$-th frequency line,*
*b) $\Psi_j^{[p]} = 0$ at frequency lines $j \pm \alpha\delta P$, $\alpha, p \in \mathbb{N}_+$,*
*c) $\psi_j^{[p]}$ has finite time-domain support of length $l_\psi^{[p]} = pN/\delta - p + 1$, i.e., $\psi_j^{[p]}[n] = 0$ for $n \geq l_\psi^{[p]}$,*
*d) $|\Psi_j^{[p+1]}| < |\Psi_j^{[p]}|$ at all but the $j$-th and $j \pm \alpha\delta$-th frequency lines.*

An example of the resulting wavelet is given below.

*Example 1. Let $N = 500, P = 1, \delta = 5$. The corresponding wavelets $\psi_{20}^{[2]}, \psi_{20}^{[3]}$ are shown in Fig. 3. The wavelets*

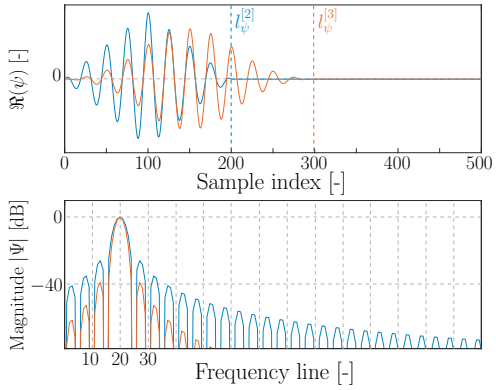


Fig. 3. Wavelets $\psi_{20}^{[2]}$ (—) and $\psi_{20}^{[3]}$ (—) in the time- (*top*) and frequency-domain (*bottom*). The wavelets extract frequency-information around the frequency line 20, within the finite wavelet duration $l_\psi^{[2]} = 199, l_\psi^{[3]} = 298$.

*approximately extract local frequency-information around the $j$-th frequency line within a local time-domain window of $l_\psi^{[2]} = 199, l_\psi^{[3]} = 298$ samples, see properties a) and c) in Def. 2. Increasing $p$ lowers the time-domain localization accuracy but improves the frequency-domain accuracy, see properties c) and d), respectively.*

A crucial property of the wavelets in Def. 2 is that their support in the time domain is compact. This enables confining the effect of the missing samples in the data $z^{\mathrm{m}}$ in the transform $\xi_j^{\mathrm{m}}$. Precisely, the samples $\xi_j^{\mathrm{m}}[v]$ that are unaffected by the missing samples are given by $v \in \mathcal{D}^{[e,p]}$, where $\mathcal{D}^{[e,p]} = \bigcap_{i=1}^{n_m} \mathcal{D}_i^{[e,p]}$ with

$$\begin{aligned}\mathcal{D}_i^{[e,p]} = \big\{ & v \in \mathbb{N} : \max(w_{\mathrm{m}}^{[e]}[i] - NP + l_\psi^{[p]}, 0) \le v < w_{\mathrm{m}}^{[e]}[i] \\ & \text{or } \min(w_{\mathrm{m}}^{[e]}[i] + l_\psi^{[p]}, NP) \le v < NP \big\},\end{aligned} \tag{9}$$

and where $w_{\mathrm{m}}^{[e]} \in \mathbb{N}^{n_{\mathrm{m}}^{[e]}}$ contains the indices of the $n_m^{[e]}$ missing samples in the $e$-th experiment. This concept is exemplified below.

*Example 2. Consider the SISO system $G_z$ with FRF shown in (—) in Fig. 2(c). The system is periodically excited with $N = 1200$ and $P = 5$ in open-loop at frequency lines $j = 10, 30, \ldots, 2990$. The output is measured without noise, but with samples $1200, \ldots, 1250$, and $3000, \ldots, 3100$ missing. The transforms $\xi_j^{\mathrm{m}}$ for wavelets with $p = 2, \delta = 2$ are illustrated in Fig. 2(c). The effect of the missing samples is confined within the (■) part.*

The main result is that the transforms $\xi_j^{\mathrm{m}}[v]$ for $v \in \mathcal{D}$ shown in (■) in Fig. 2(c) provide a time-frequency representation of the data $z^{\mathrm{m}}$ that is fully unaffected by the missing samples. This is exploited in the selection of $\bar{M}$ in (5) in the following.

### 3.2.3. Selection of matrix $\bar{M}$

To pose the regression (5) in the time-frequency plane, the matrix $\bar{M}$ is selected as $\bar{M} = \mathrm{blkdg}(\bar{M}^{[1]}, \ldots, \bar{M}^{[n_u]})$, where $\bar{M}^{[e,p]} = \begin{bmatrix} M_{\bar{k}_0}^{[e,p]}, \ \ldots, \ M_{\bar{k}_{\bar{N}-1}}^{[e,p]} \end{bmatrix}$ with

$$\bar{M}_{\bar{k}_j}^{[e,p]} = \mathrm{diag}(\Psi_{\bar{k}_j}^{[p]}) \mathcal{H} \mathcal{W}^{[e,p]}. \tag{10}$$

The operation (10) reflects the time-frequency plane transformation in (8) around a $\tilde{k}_j$-th frequency line, with the additional selection matrix $\mathcal{W}^{[e,p]}$.

The main mechanism to achieve an exact estimator (6) in the sense of Theorem 1 is to discard the affected samples $v$ in the transform $\xi_j^{\mathrm{m}}[v]$, recall the part in (■) in Fig. 2(c). This is achieved by selecting the matrix $\mathcal{W}^{[e,p]}$ in (10) as

$$[\mathcal{W}^{[e,p]}]_{v,v} = \begin{cases} 1 \text{ if } v \in \mathcal{D}^{[e,p]} \\ 0 \text{ otherwise} \end{cases}, \tag{11}$$

for $v = 0, \ldots, NP-1$ and where $\mathcal{D}^{[e,p]}$ is the set in (9). The specific selection of the wavelet parameters $\{\tilde{k}, \delta, p\}$ depends on the selected model parametrization $\{K_{\bar{k}_j}, \Theta_{\bar{k}_j}\}$ in (5). This parametrization is presented next.

## 3.3 Local Polynomial Model Parametrization

In this section, the model parametrization in $\{K_{\bar{k}_j}, \Theta_{\bar{k}_j}\}$ in (5) is specified. The local polynomial parametrization as used in LPM for periodic excitations (Pintelon et al., 2011) is used as basis. These local concepts are extended to a global formulation to allow for incorporation of the wavelet-based transform reflected by matrix $\bar{M}$ in (10).

### 3.3.1. Parametrization in local frequency window

Given periodic excitation signals $w$, a distinction is made between the excited frequency (EF) lines and the non-excited frequency (NEF). The DFT $W$ in (1) contains energy only at the EF lines $\bar{k} = \begin{bmatrix} \bar{k}_0, \ \ldots, \ \bar{k}_{\bar{N}-1} \end{bmatrix}$, where $\bar{k}_j = j\gamma P$ with $j = 0, \ldots, \lfloor N/\gamma \rfloor - 1$. Herein, $\gamma \in \mathbb{N}_+$ is a excitation design parameter that controls the sparsity of the excitation grid.

At the NEF lines $\bar{k} + q$, with $q = [1, 2, \ldots, \gamma P - 1]$, the frequency response $G_z(\Omega_k)W(k)$ equals zero, see Fig. 4. Hence, at the NEF lines, $Z$ in (1) reduces to

$$Z(\bar{k}_j + q) = T(\Omega_{\bar{k}_j + q}) + N_{z_{\mathrm{st}}}(\bar{k}_j + q), \tag{12}$$

where $T = T_z + T_h$ lumps the transient of the system $G_z$ and the noise dynamics $H_z$. The transient $T$ is a smooth function of the frequency. In a local frequency window, it can be approximated by $(R+1)$-th order polynomials,

$$T^{[e]}(\Omega_{\bar{k}+q}) = T^{[e]}(\Omega_{\bar{k}}) + \sum_{s=1}^{R} t_s^{[e]}(\bar{k}) q^s + \mathcal{O}^{[e]}(q), \tag{13}$$

where $\mathcal{O}(q) = (1/\sqrt{NP})\mathcal{O}\left((q/NP)^{R+1}\right)$ is the remainder of an $(R+1)$-th order Taylor series approximation around $T^{[e]}(\Omega_{\bar{k}})$, see Pintelon et al. (2010). At the EF lines, the output is given by

$$Z(\bar{k}_j) = G_z(\Omega_{\bar{k}_j})W(\bar{k}_j) + T(\Omega_{\bar{k}_j}) + N_{z_{\mathrm{st}}}(\bar{k}_j), \tag{14}$$

The $n_\Theta = n_z n_u (R+2)$ estimation parameters around the $j$-th EF line are collected in the vector

$$\Theta_{\bar{k}_j} = \left[ G_z(\Omega_{\bar{k}_j}), \ \Theta_T^{[1]}(\bar{k}_j), \ \ldots, \ \Theta_T^{[n_u]}(\bar{k}_j) \right] \in \mathbb{C}^{n_z \times n_u(R+2)}, \tag{15}$$

with $\Theta_T^{[e]}(\bar{k}_j) = \left[ T^{[e]}(\Omega_{\bar{k}_j}), \ t_1^{[e]}(\bar{k}_j), \ \ldots, \ t_R^{[e]}(\bar{k}_j) \right]$. Combining (13) - (15), $Z$ is expressed at the $n_r$ frequency lines $\bar{k}_j + r$, with $r = [-\gamma P + 1, -\gamma P + 2, \ldots, \gamma P - 1]$ as

$$Z(\bar{k}_j + r) = \Theta_{\bar{k}_j} K_{\bar{k}_j}(r) + N_{z_{\mathrm{st}}}(\bar{k}_j + r) + \mathcal{O}(r), \tag{16}$$

where $Z(\bar{k}_j + r)$ is structured as

$$Z(\bar{k}_j + r) = \left[ Z^{[1]}(\bar{k}_j + r), \ldots, Z^{[n_u]}(\bar{k}_j + r) \right].$$

The regressor in (16) is given by

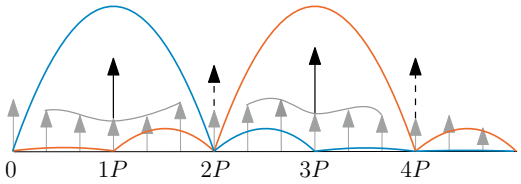


Fig. 4. Frequency-domain representation of $Z$ in (1) for $P = 3, \gamma = 1$ without noise. At the EF lines $[1P, 2P, 3P, 4P]$, the response consists of the transient (grey arrows) and periodic response (black arrows). At the remaining NEF lines, the response contains only transient contributions. The grey curves represent the local transient estimates based on the $n_r$ lines around the $[1P, 3P]$ odd EF lines. The frequency-domain weights introduced by $\Psi_{1P}$ and $\Psi_{3P}$ are shown in (—) and (—).

$$K_{\bar{k}_j}(r) = \begin{bmatrix} W(\bar{k}_j + r) \\ I_{n_u} \otimes \begin{bmatrix} r^0 \\ \vdots \\ r^R \end{bmatrix} \end{bmatrix} \in \mathbb{C}^{n_u(R+2) \times n_u(2\gamma P - 1)}. \quad (17)$$

The obtained parametrization $\{K_{\bar{k}_j}, \Theta_{\bar{k}_j}\}$ describes the frequency response in a local frequency window around the EF line $\bar{k}_j$. To enable handling the global frequency-domain impact of the missing samples, the parametrization is extended to a global parametrization $\{\bar{K}, \bar{\Theta}\}$ next.

### 3.3.2. Constructing the global regressor

In loose terms, the global regressor $\bar{K}$ in (5) is obained by stacking the local matrices $K_{\bar{k}_j}(r)$ in (17), such to span all $NP$ frequency lines. Precisely, it is composed as $\bar{K} = \left[\bar{K}^{[1]}, \ldots, \bar{K}^{[n_u]}\right]$, where

$$\bar{K}^{[e]} = \begin{bmatrix} 0_{\frac{1}{2}n_{\bar{\Theta}} \times 1}, & \tilde{K}^{[e]}, & 0_{\frac{1}{2}n_{\bar{\Theta}} \times 1}, & \mathrm{conj}(\tilde{K}^{[e]})\mathcal{I} \\ 0_{\frac{1}{2}n_{\bar{\Theta}} \times 1}, & i\tilde{K}^{[e]}, & 0_{\frac{1}{2}n_{\bar{\Theta}} \times 1}, & -i\mathrm{conj}(\tilde{K}^{[e]})\mathcal{I} \end{bmatrix} \in \mathbb{C}^{n_{\bar{\Theta}} \times NP} \quad (18)$$

where $\mathcal{I}$ is a $(\frac{1}{2}NP-1)$-dimensional exchange matrix, and $\tilde{K}^{[e]} \in \mathbb{C}^{\frac{1}{2}n_{\bar{\Theta}} \times \frac{1}{2}NP-1}$ is composed of the local matrices $K_{\tilde{k}_j}(r) = \left[K^{[1]}_{\tilde{k}_j}(r), \ldots, K^{[n_u]}_{\tilde{k}_j}(r)\right]$ in (17) as

$$[\tilde{K}^{[e]}]_{c_j, \tilde{k}_j + r - 1} = K^{[e]}_{\tilde{k}_j}(r), \quad (19)$$

with $\tilde{k} = [\tilde{k}_0, \ldots, \tilde{k}_{\tilde{N}-1}] \subset \bar{k}$ and row index $c_j = [jn_\Theta, jn_\Theta + 1, \ldots, (j+1)n_\Theta - 1]$. The associated $n_{\bar{\Theta}} = 2\tilde{N}n_\Theta$ parameters $\bar{\Theta}$ in (5) are collected in

$$\bar{\Theta} = \left[\Re\left[\Theta_{\tilde{k}_0} \ \ldots \ \Theta_{\tilde{k}_{\tilde{N}-1}}\right] \ \Im\left[\Theta_{\tilde{k}_0} \ \ldots \ \Theta_{\tilde{k}_{\tilde{N}-1}}\right]\right]. \quad (20)$$

The result of the parametrization $\{\bar{K}, \bar{\Theta}\}$ in conjunction with $\bar{M}$ in (10) is that the estimator (6) yields a exact estimate of $\bar{\Theta}$ in the absence of noise $N_z$ and remainders $\bar{O}$. Exploiting (20), (15) and (2), the open-loop plant estimate $\hat{G}(\Omega_{\bar{k}_j})$ is obtained from $\hat{\bar{\Theta}}$ via

$$\hat{G}(\Omega_{\bar{k}_j}) = \hat{G}_y(\Omega_{\bar{k}_j})\hat{G}_u^{-1}(\Omega_{\bar{k}_j}). \quad (21)$$

### 3.3.3. Selection of parameters $\{\tilde{k}, \delta, p\}$

The selection of the parameters $\{\tilde{k}, \delta, p\}$ plays an important role in trading off between variance errors due to noise $N_z$ and bias errors due to remainders $\bar{\mathcal{O}}$ (Dirkx et al., 2022). The following selection balances between the two criteria. The selection divides the identification problem into two separate subproblems.

The first subproblem is aimed at estimation at the odd EF lines by setting $\tilde{k} = \tilde{k}_{\text{odd}} := \gamma P[1, 3, \ldots, \frac{N}{2\gamma} - 1]$. Additionally, $\delta = \gamma$ is selected, which makes the zeros of $\Psi^{[p]}_{\tilde{k}}$ coincide with all EF lines outside the current local window, as shown in Fig. 4. The result is fourfold: 1) it emphasizes $G_z$ and the transient $T_z$ locally around the selected odd EF line, 2) it suppresses the contributions from the other frequency lines, 3) it eliminates the contributions from all other EF lines, and 4) this is achieved for the largest $\mathrm{card}(\mathcal{D}^{[e,p]})$. In a similar procedure, the second subproblem is aimed at estimating $\hat{G}$ at the even EF lines $\tilde{k}_{\text{even}} := \gamma P[2, 4, \ldots, \frac{N}{2\gamma}]$.

The wavelet parameter $p$ provides a further tuning variable to control the trade-off between bias and variance errors. Increasing $p$ reduces bias at the expense of larger variance, see Dirkx et al. (2022) for more details.

### 3.4 Variance estimation

In this section, the frequency-domain localization properties of the wavelet are exploited to estimate the noise-induced variance errors in the estimated plant model $\hat{G}$ from the measured incomplete data $Z^{\mathrm{m}}$.

*Theorem 3. Let the wavelet DFT $\Psi_{\tilde{k}_j}$ be decomposed as*

$$\Psi_{\tilde{k}_j} = \Psi^0_{\tilde{k}_j} + \Psi^\Delta_{\tilde{k}_j} \quad (22)$$

*where $\Psi^0_{\tilde{k}_j}$ is defined as*

$$[\Psi^0_{\tilde{k}_j}]_n = \begin{cases} [\Psi_{\tilde{k}_j}]_n & \text{if } n \in (\tilde{k}_j + r) \\ 0 & \text{otherwise} \end{cases} \quad (23)$$

*and where $\Psi^\Delta_{\tilde{k}_j}$ is the remainder, defined by (22) and (23). Let the following assumptions hold:*

- *i) The remainders $\bar{\mathcal{O}}$ in (5) are zero,*
- *ii) The noise DFT $N^{[e]}_{z_{\text{st}}}$ has a uniform magnitude over the frequency lines $\tilde{k}_j + r$, with covariance $C_{z_{\tilde{k}_j}}$,*
- *iii) The wavelet remainder $\Psi^\Delta_{\tilde{k}_j}$ in (22) is negligible.*

*Let $M_{\tilde{k}_j} := \mathrm{blkdg}(M^{[1]}_{\tilde{k}_j}, \ldots, M^{[n_u]}_{\tilde{k}_j})$. Then, the noise covariance is related to the weighted residual error $R_{\tilde{k}_j} := (Z^{\mathrm{m}} - \hat{\bar{\Theta}}\bar{K})M_{\tilde{k}_j}$ as*

$$C_{z_{\tilde{k}_j}} = \frac{1}{\mathrm{Tr}(\mathcal{P}M_{\tilde{k}_j}M^H_{\tilde{k}_j}\mathcal{P}^H)}\mathbb{E}\left\{R_{\tilde{k}_j}R^H_{\tilde{k}_j}\right\}, \quad (24)$$

*with $\mathcal{P} = (I - \frac{1}{2}\bar{B}\bar{K}^H\left(\Re(\bar{K}\bar{B}\bar{K}^H)\right)^{-1}\bar{K})$.*

The proof is omitted to conserve space. Thm. 3 extends the procedure in the classical LPM (Pintelon et al., 2010) to the estimation from incomplete data in the estimator (6). Expression (24) typically yields an accurate covariance estimate, since assumption ii) in Thm. 3 holds approximately in a local window. Assumption iii) is approximately satisfied for frequency-domain localizing wavelets. Assumption i) holds approximately by suitable choice of $R$.

The covariances in the estimated closed-loop transfer functions $G_z$ are estimated via the mapping

$$C_{\mathrm{vec}(\hat{G}_z)}(\tilde{k}_j) = \frac{1}{2}\mathrm{conj}(S^H_{\tilde{k}_j}S_{\tilde{k}_j}) \otimes C_{z_{\tilde{k}_j}}, \quad (25)$$

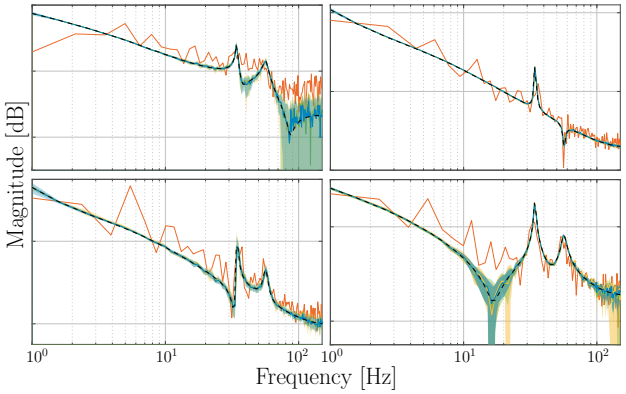


Fig. 5. The time-frequency plane estimators for $p = 1$ (—), $p = 2$ (—), and $p = 3$ (—) generate accurate FRMs of the true system $G$ (- -), in contrast to the classical LPM (—). The 95% confidence regions (shaded) increase for an increasing value of $p$.

where

$$S_{\tilde{k}_j} = \begin{bmatrix} \Re(\bar{B}\bar{K}^H) \\ -\Im(\bar{B}\bar{K}^H) \end{bmatrix} (\Re(\bar{K}\bar{B}\bar{K}^H))^{-1} \left( s \otimes \begin{bmatrix} I_{n_u} \\ 0_{n_\Theta - n_u \times n_u} \end{bmatrix} \right)$$

and $s = [1 \;\; i]^T \otimes \left[\delta_{0,j}, \ldots, \delta_{N_{\tilde{k}-1},j}\right]^T$, with $\delta_{a,b}$ the Kronecker delta. The mapping (25) is similar to Pintelon and Schoukens (2012, Ch. 7). The mapping from the closed-loop FRM $\hat{G}_z$ to the open-loop system $\hat{G}$ is done according to (Pintelon and Schoukens, 2012, Ch. 7),

$$C_{\mathrm{vec}(\hat{G})} = (\hat{G}_u^{-1} \otimes \begin{bmatrix} I_{n_y} & -\hat{G} \end{bmatrix}) C_{\mathrm{vec}(\hat{G}_z)} (\hat{G}_u^{-1} \otimes \begin{bmatrix} I_{n_y} & -\hat{G} \end{bmatrix})^H,$$

wherein the index $\tilde{k}_j$ is omitted.

## 4. SIMULATION STUDY

### 4.1 Simulation setup

The time-frequency plane LPM is applied to a $2 \times 2$ simulation model $G$, with 2 highly damped modes, and 2 lightly damped modes, with FRM shown in (- -) in Fig. 5. The system is closed-loop controlled by a PID-type feedback controller. Random phase periodic excitations with uniform spectrum and $P = 5$, $N = 2000$, $\gamma = 2$ are used. The sampling time is $T_s = 0.02$s and a total number of 500 samples are missing per experiment. The outputs $z$ are perturbed by white noise $\nu_y$. Due to slow dynamics of the highly damped modes, a significant transient is present in the output $z$ over the duration of the experiments.
The time-frequency plane LPM estimator is evaluated for the values $p = 1, 2, 3$ and $R = 2$ and compared to the classical LPM.

### 4.2 Identification results

The identified FRM models and their estimated 95% confidence region bounds are shown in Fig. 5, together with the true system (- -). The classical LPM (—) delivers a poor model. The estimates from the time-frequency plane LPM accurately represent the true dynamics. The uncertainty bound increases for increasing values of $p$. This is supported by the error decomposition for different values of $p$ in Fig. 6. Clearly, bias is reduced for increasing values of $p$. Concludingly, the observations are in line with the statements in Sec. 3.3.3 and demonstrate good performance of the presented techniques.

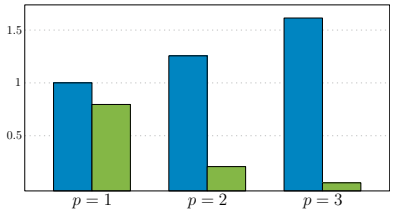


Fig. 6. Variance ( ■ ) and bias ( ■ ) contributions in the model error for $p = 1, 2, 3$. The values are equally scaled such that the variance for $p = 1$ equals one.

## 5. CONCLUSIONS

The presented identification algorithm enables accurate FRM estimation from incomplete data records. This is achieved by employing a wavelet-based transform to obtain a data representation in the time-frequency plane, in which the effect of the missing samples in the time domain is separated from the system characteristics in the frequency domain. The time- and frequency domain localization properties of the wavelets enable low-bias estimates and give rise to a variance estimation procedure. This is supported by results from a simulation study, in which good identification performance is confirmed.

## REFERENCES

Barbé, K., Van Moer, W., Lauwers, L., and Björsell, N. (2012). A simple nonparametric preprocessing technique to correct for nonstationary effects in measured data. *IEEE Trans. Instrum. Meas.*, 61(8), 2085–2094.

Daubechies, I. (1990). The wavelet transform, time-frequency localization and signal analysis. *IEEE Trans. Inf. Theory*, 36(5), 961–1005.

Dirkx, N., Tiels, K., and Oomen, T. (2022). Frequency response function identification from incomplete data: A wavelet-based approach. *IFAC-PapersOnLine*, 55(37), 439–444. 2nd Modeling, Estimation and Control Conference MECC 2022.

Dirkx, N., Tiels, K., and Oomen, T. (2023). A wavelet-based approach to FRF identification from incomplete data. *IEEE Trans. Instrum. Meas.*

Gröchenig, K. (2001). *Foundations of time-frequency analysis*. Springer Science & Business Media.

Kar, S. and Moura, J.M. (2009). Distributed consensus algorithms in sensor networks: Quantized data and random link failures. *IEEE Trans. Signal. Process.*, 58(3), 1383–1400.

Pintelon, R. and Schoukens, J. (2012). *System identification: a frequency domain approach*. John Wiley & Sons.

Pintelon, R., Schoukens, J., Vandersteen, G., and Barbé, K. (2010). Estimation of nonparametric noise and FRF models for multivariable systems—part I: Theory. *Mech. Syst. Signal. Process.*, 24(3), 573–595.

Pintelon, R., Vandersteen, G., Schoukens, J., and Rolain, Y. (2011). Improved (non-) parametric identification of dynamic systems excited by periodic signals—the multivariate case. *Mech. Syst. Signal. Process.*, 25(8), 2892–2922.

Schoukens, J., Vandersteen, G., Barbé, K., and Pintelon, R. (2009). Nonparametric preprocessing in system identification: a powerful tool. In *2009 Eur. Control Conf. (ECC)*, 1–14. IEEE.

Schoukens, J., Vandersteen, G., Rolain, Y., and Pintelon, R. (2012). Frequency response function measurements using concatenated subrecords with arbitrary length. *IEEE Trans. Instrum. Meas.*, 61(10), 2682–2688.

Stoica, P., Li, J., Ling, J., and Cheng, Y. (2009). Missing data recovery via a nonparametric iterative adaptive approach. In *2009 IEEE International Conference on Acoustics, Speech and Signal Processing*, 3369–3372.

Ugryumova, D., Pintelon, R., and Vandersteen, G. (2014). Frequency response function estimation in the presence of missing output data. *IEEE Trans. Instrum. Meas.*, 64(2), 541–553.